A multi-layer integral model for locally-heated thin film flow

E. D. Kay[1], S. Hibberd[b], H. Power[a,*]

[a] *Department of Mechanical, Materials and Manufacturing Engineering, University of Nottingham, Nottingham, NG7 2RD, UK*
[b] *School of Mathematical Sciences, University of Nottingham, Nottingham, NG7 2RD, UK*
[c] *Norton Straw Consultants, The Steam Engine House, Darley Abbey Mills, Derby, DE22 1DZ, UK*

Abstract

Based on an approach used to model environmental flows such as rivers and estuaries, we develop a new multi-layered model for thin liquid film flow on a locally-heated inclined plane. The film is segmented into layers of equal thickness with the velocity and temperature of each governed by a momentum and energy equation integrated across each layer individually. Matching conditions applied between the layers ensure the continuity of down-plane velocity, temperature, stress and heat flux. Variation in surface tension of the liquid with temperature is considered so that local heating induces a surface shear stress which leads to variation in the film height profile (the Marangoni effect). Moderate inertia and heat convection effects are also included.

In the absence of Marangoni effects, when the film height is uniform, we test the accuracy of the model by comparing it against a solution of the full heat equation using finite differences. The multi-layer model offers significant improvements over that of a single layer. Notably, with a sufficient number of layers, the solution does not exhibit local regions of negative temperature often predicted using a single-layer model.

With Marangoni effects included the film height varies however we find heat convection can mitigate this variation by reducing the surface temperature gradient and hence the surface shear stress. Numerical results corresponding to the flow of water on a vertical plane show that very thin films are dominated by the Marangoni shear stress which can be sufficiently strong to overcome gravity leading to a recirculation in the velocity field. This effect reduces with increasing film thickness and the recirculation eventually disappears. In this case heating is confined entirely to the interior of the film leading to a uniform height profile.

Keywords: Thin film flow, Marangoni effect, layered model, integral model, moderate Reynolds number

1. Introduction

Thin liquid film flows appear in a wide range of physical settings. In engineering they are used in heat exchangers, to cool surfaces, to provide lubrication between moving parts, to coat surfaces and to remove oil slicks from the sea. The tear film in the eye and mucus linings of the airways are biological examples. Two review papers [1, 2] provide an expansive list of applications and theory - both of which are the continually developing. A good deal of research into thin film flow was driven by the photographic film making industry where the production process contains various film flows including dynamic wetting lines, fluid withdrawal from pools, flow over inclined planes, rimming and coating flows, falling liquid curtains and metering from small gaps. The review by [3] discusses these in detail.

The model we derive in this paper is applicable to thin film flows generally but we present it for flow down an inclined plane which is an extensively studied problem appearing in many applications. The multilayer aspect of our work refers to the modelling approach rather than to stratified films of different fluids however there are features shared by both and so we note a few examples.

A key historical paper on two-layer flow is by Yih [4] who examined the stability of two-layer viscosity-stratified flow in a horizontal channel, extending the work of Benjamin who studied a single-layer film with free surface [5]. Further stability analysis of the inclined channel [6] and the effects of a surfactant at the interface [7] have been made. The presence of a rigid upper boundary is found to have a strong effect on the stability of multilayer channels compared to those with a free upper surface. The presence of a free upper surface can lead to instability even in the limit of vanishing Reynolds number in contrast to the channel flow case [8]. Extension of the free surface problem to include surfactants [9] and evaporation [10] has also been carried out . Focussing on the industrial

*Corresponding author
Email address: henry.power@nottingham.ac.uk (H. Power)

application to coating and extrusion, the inertia-less case of a general n-layer film has been studied [11] and it is found that the upper layer properties have the most pronounced effect on film height profiles.

In these studies, as with many thin film models, lubrication theory is used. Here inertial effects are neglected or appear as a small perturbation to the leading order Stokes flow balance between gravity and viscosity. For instances when inertial and heat convection effects are important, such as in fast-moving films, the lubrication theory approximation is no-longer suitable and it is appropriate to use an Integral Boundary Layer (IBL) approach. Here the Navier–Stokes equations are integrated through the depth of the film becoming valid in an average sense across the film. The variations in velocity and temperature across the film is approximated by a profile which is usually chosen as a low-order polynomial. This method reduces by one the dimension of the problem and is equivalent to the Kármán–Pohlhausen method for boundary layers [12].

Modelling of this type for film flows is associated with Shkadov [13] who, using a quadratic velocity profile, studied the growth of disturbances on the surface of free-falling films. His model comprised two coupled conservation equations for mass and momentum which were solved to give a film height profile and local film volume flux. Such two-equation models were found to rectify shortcomings, such as finite-time blow-up, of earlier modelling strategies based on solving a single evolution equation for film height to which the local volume flux was completely enslaved [14]. These have been applied to industrial flows such as the making of photographic film [15, 16].

An obvious approach to improve Shkadov-type models is to use higher-order polynomials. Models based on the weighted-average technique with sixth-order polynomials for velocity [17] show improvements in stability predictions over the original quadratic model of Shkadov. Extensions to include thermal effects within IBL models have been provided by [18] and [19] for a linear temperature profile and [20] for a quadratic temperature profile. A shortcoming of these models has been the prediction of areas of the film with unphysical negative temperatures when convection effects are significant.

Prior to their applications to thin films, IBL models have been used for ocean wave, fluvial and estuarine modelling (see the 18th century works of [21] and [22]). Improvement in the flow field resolution for these environmental flows has generally arisen from (i) using

higher-order polynomials [23], which is essentially the strategy applied to thin film flows in [17] and by co-workers, or (ii) using a multi-layer approach, e.g. [24, 25, 26, 27]. In the multi-layer approach the flow thickness is divided into a series of layers, each modelled using an IBL approximation with low-order polynomial profile. For estuarine flows this has allowed Boussinesq-type models for wave propagation to be used in far deeper waters than would be accurate using a single-layer model [25]. This extended capability has motivated our application the approach to thin films where single-layer models have been successful but have exhibited limitations arising from approximating a complex flow with a low-order polynomial.

One approach to multi-layered models is to have the inter-layer boundaries coincident with the streamlines of the flow giving zero mass flux between the layers. This yields a simplified set of governing equations and is particluarly relevant in the case of gradually-varying uni-directional flow where interlayer fluxes are small, or of layers of immiscible fluids where there is no mass exchange [28]. When there is significant mixing between layers, or if recirculations are present, an alternative approach with layer boundaries located independent of the flow field (for example layers uniformly distributed through depth) and inter-layer fluxes accounted for by matching conditions between the flows in each layer is needed. This approach has been adopted by, for example, Audusse and co-workers [29, 26, 27]

In this paper we apply a multi-layer IBL approach including inter-layer fluxes to thin film flow. With most multi-layer models being applied to environmental flows, this is a novel application for which the authors are not aware of any previous work. The physical setting for our model is steady thin film flow down a locally-heated inclined plane. The surface tension coefficient of the film varies with temperature so that local heating induces shear stress at the surface (the Marangoni effect) which creates a non-uniform film height profile. Accurate resolution of the surface temperature gradient is important in order to capture the Marangoni effect correctly. It is noted that single-layer IBL models for these flows have reported unphysical negative temperatures on the film surface [18, 20] leading to inaccuracy in the resulting film profile. Adaption of the multi-layer IBL approach to this thin film application gives significant improvements in the local temperature fields and hence surface temperature gradient resolution.

As described, thin film models tend to be cast in terms of the film thickness (and other average variables if the model is to also include the effects of temperature or a dissolved solute) so that the location of the free surface arises as a solution of the model. This avoids working in a computational domain of initially-unknown shape. However numerical solutions to the full Navier–Stokes equations, solved in a domain with deforming free-surface have been carried out. In [30] stratified film flow of two different liquids down a vertical plate with one layer injected beneath the other from a slot in the plane is simulated. Here the full Navier–Stokes equations are solved with appropriate boundary conditions applied at the deforming interface between layers and at the free surface. Alternatively the Volume of Fluid (VOF) method, popular in multiphase CFD, may be used to obtain the film surface by solving a convection equation for an indicator function as recently examined in numerical experiments of vertically-falling films[31].

The structure of the paper is as follows: In section 2 we formulate the steady layered model for film flow and temperature and describe the numerical solution method. In section 3 we consider films of uniform height and compare the layered model to a full numerical solution of the temperature field over the rectangular domain of the film. In section 4 we consider cases where Marangoni effects induce a variation in film height and investigate how the number of layers used affects the results. Section 5 details a numerical investigation with fixed liquid and plane geometry. Conclusions in section 6 evaluate both the physical and numerical aspects of this new multi-layered approach to modelling thermal effects in thin film flows.

2. Model formulation

2.1. Governing equations for film flow

The model is for the steady two-dimensional gravity-driven flow of a thin film of liquid down an inclined plane which makes an angle α with the horizontal, as illustrated in figure 1. The liquid has density ρ, kinematic viscosity ν, specific heat c and thermal diffusivity κ. A section of the planar substrate is heated to a temperature $\hat{T}_\infty + \Delta\hat{T}$, where $\hat{T}_\infty$ is the temperature of the unheated substrate. Gas which overlies the film is at pressure $\hat{p}_a$ and has temperature $\hat{T}_\infty$. Far from the heated section the film temperature is uniformly $\hat{T}_\infty$. The liquid-gas interface has a heat transfer coefficient Γ and surface

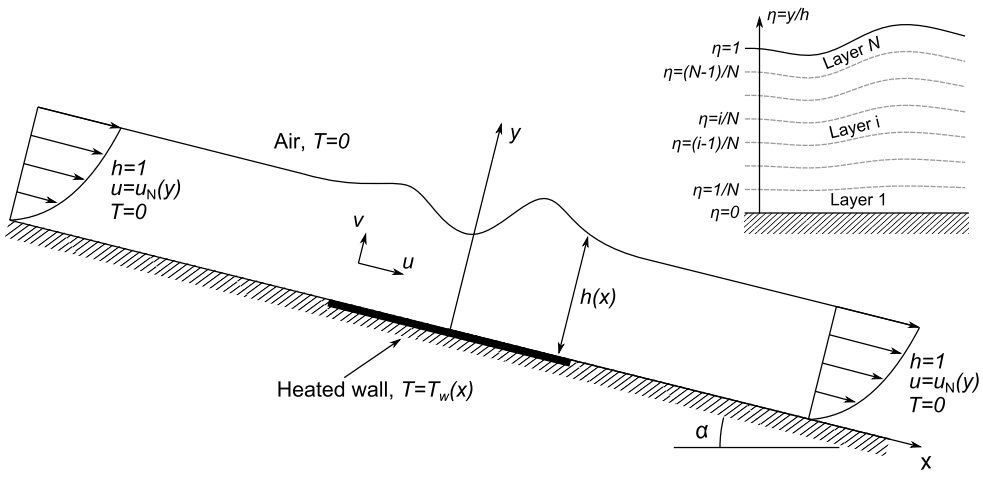

Figure 1: Schematic of the film flowing over a locally heated inclined plane and the labelling and position of layer interfaces.

tension coefficient σ which is taken to vary linearly with temperature $\hat{T}$ according to the relationship $\sigma = \sigma_0 - \sigma_T(\hat{T} - \hat{T}_\infty)$. Here the constant σ_0 is the surface tension coefficient at the reference temperature $\hat{T}_\infty$ and σ_T (also constant) is the variation in surface tension with temperature.

This effect lowers the surface tension in the vicinity of the heated region, creating a Marangoni stress which leads to a non-uniform film height profile. Far from the heated section there is no Marangoni effect and the film height is uniformly h_0 and the flow velocity is parallel to the plane with profile given by the Nusselt solution

$$\hat{u}_{\mathrm{NU}}(\hat{y}) = \frac{g \sin\alpha}{\nu}(h_0\hat{y} - \tfrac{1}{2}\hat{y}^2). \tag{1}$$

Here $\hat{y}$ measures distance normal to the plane and g is the acceleration due to gravity. A convenient characteristic velocity of the film is it's mean value

$$\hat{U}_0 = \frac{1}{3} g \sin\alpha / \nu h_0^2. \tag{2}$$

To model the non-uniform film height profile driven by Marangoni effects, we adopt a thin film approximation with small parameter $\epsilon = h_0/l$ where l is the characteristic

length of the heated section. The $\hat{x}$ coordinate is scaled by l, the $\hat{y}$ coordinate by h_0, the $\hat{x}-$component of velocity by $\hat{U}_0$ and the $\hat{y}-$ component of velocity by $\epsilon\hat{U}_0$. The dimensionless temperature field T is introduced such that $\hat{T} = \hat{T}_\infty + T\Delta\hat{T}$. To include moderate inertial effects, the pressure $\hat{p}$ is scaled on the dynamic pressure so that $\hat{p} = \hat{p}_a + \rho\hat{U}_0^2 p$ for p the dimensionless pressure field. In addition to α and ϵ, the problem gives rise to the Reynolds, Péclet, Biot, Marangoni and Weber numbers, defined respectively as

$$Re = \frac{g\sin\alpha h_0^3}{3\nu^2}, \quad Pe = \frac{g\sin\alpha h_0^3}{3\nu\kappa}, \quad Bi = \frac{h_0\Gamma}{\rho c\kappa}, \quad Ma = \frac{3\sigma_T\Delta\hat{T}}{\rho g\sin\alpha h_0^2}, \quad We = \frac{3^2\sigma_0\nu^2}{\rho g^2 h_0^5\sin^2\alpha}. \tag{3}$$

Leading-order equations for the film velocity and temperature are obtained from a long-wavelength approximation of the Navier-Stokes and energy equations:

$$\partial_x u + \partial_y v = 0, \tag{4}$$

$$R\left[\partial_x(u^2) + \partial_y(vu)\right] = -3\epsilon\cot\alpha h' + Ch''' + 3 + \partial_{yy}u, \tag{5}$$

$$P\left[\partial_x(uT) + \partial_y(vT)\right] = \partial_{yy}T + \epsilon^2\partial_{xx}T. \tag{6}$$

The Reduced Reynolds, Péclet, Marangoni and capillary numbers are defined $R = \epsilon Re$, $P = \epsilon Pe$, $M = \epsilon Ma$ and $C = \epsilon^3 WeRe$ respectively. A superscript prime denotes a total derivative taken with respect to x, e.g. $h' = dh/dx$, and partial derivatives are denoted by, for example, $\partial_x = \partial/\partial x$. In obtaining (5)-(6) we have retained all leading-order terms under the assumption that the reduced Reynolds and Péclet numbers R and P are $O(1)$ so inertial and heat-convection effects are included. An expression for the film pressure field $p = \{3\epsilon\cot\alpha(h-y) - Ch''\}/R$ is obtained by integrating the long-wavelength approximation of the $y-$momentum equation and applying the free surface pressure condition $p(y=h) = -Ch''/R$ which encodes the effects of surface tension. This is substituted into the pressure gradient term in the $x-$momentum equation which yields the first two terms on the right-hand side of (5). As is standard for thin film flows [18] we take $C = O(1)$ to retain surface tension effects which may become significant when the film height profile varies rapidly making h''' large. For the same reason the $x-$pressure gradient term in (5) is retained though it appears multiplied by ϵ. On similar grounds we retain the x-diffusion term in (6) though it appears multiplied by ϵ^2 since this can be significant in regions where the temperature field varies rapidly [20].

Equations (4)-(6) are supplemented by a kinematic condition, Marangoni stress and Newton's law of cooling at the gas-liquid interface $y = h(x)$ giving respectively:

$$uh' = v, \tag{7}$$

$$\partial_y u + M\partial_x T = 0, \tag{8}$$

$$\partial_y T + BiT = 0. \tag{9}$$

On the planar surface the following no-slip, no-penetration and fixed temperature conditions apply,

$$u = v = 0, \quad T = T_w(x), \tag{10}$$

where $T_w(x)$ is a specified profile of temperature.

Far upstream and downstream of the locally-heated section the film is isothermal with the Nusselt velocity profile (1). The following dimensionless far-field conditions apply:

$$h = 1, \tag{11}$$

$$u(y) = 3(y - y^2/2) \equiv u_{\mathrm{NU}}(y), \tag{12}$$

$$v = 0, \tag{13}$$

$$T = 0. \tag{14}$$

2.2. The multi-layered model

To formulate the multi-layered model the film is segmented into N ($N \geq 1$) layers of equal height labelled from the wall to the surface by i ($i = 1 \ldots N$). This is illustrated in figure 1. The $i-$th layer has lower- and upper-boundaries located at $y = (i-1)h/N \equiv d_{i-1}$ and $y = ih/N \equiv d_i$ respectively. We also introduce the normalized coordinate $\eta = y/h$ with $\eta = 0$ located on the plane ($y = 0$), $\eta = 1$ at the surface ($y = h$) and the interface between the layers i and $i+1$ at $\eta = i/N \equiv \eta_i$. It is important to note that except for the film surface and wall, the layer boundaries are not generally material interfaces and mass may transfer between the layers. The velocity components and temperature within each layer are denoted u_i, v_i and T_i.

In terms of the scaled co-ordinate η, the boundary conditions at the free surface

(7)-(9) and wall (10) are written

$$u_N h' = v_N \qquad \text{at } \eta = 1 \quad \text{(kinematic free-surface condition)}, \tag{15}$$

$$\frac{\partial u_N}{\partial \eta} + Mh\frac{\partial T_N}{\partial x} = 0 \qquad \text{at } \eta = 1 \quad \text{(Marangoni surface shear)}, \tag{16}$$

$$\frac{\partial T_N}{\partial \eta} + BihT_N = 0 \qquad \text{at } \eta = 1 \quad \text{(surface heat transfer)}, \tag{17}$$

$$u_1 = 0 \qquad \text{at } \eta = 0 \quad \text{(no slip velocity)}, \tag{18}$$

$$v_1 = 0 \qquad \text{at } \eta = 0 \quad \text{(no penetration velocity)}, \tag{19}$$

$$T_1 = T_w(x) \qquad \text{at } \eta = 0 \quad \text{(fixed wall temeperature)}. \tag{20}$$

At the internal interfaces between each layer we specify matching conditions which ensure that u and T are continuous there:

$$u_{i+1} = u_i \qquad \text{at } \eta = i/N \text{ for } i = 1 \ldots N-1, \tag{21}$$

$$T_{i+1} = T_i \qquad \text{at } \eta = i/N \text{ for } i = 1 \ldots N-1. \tag{22}$$

The stress tensor and heat flux must be continuous across each internal layer interface which, after simplification using the thin-film approximation, gives the following matching conditions:

$$\frac{\partial u_{i+1}}{\partial \eta} = \frac{\partial u_i}{\partial \eta} \qquad \text{at } \eta = i/N \text{ for } i = 1 \ldots N-1, \tag{23}$$

$$\frac{\partial T_{i+1}}{\partial \eta} = \frac{\partial T_i}{\partial \eta} \qquad \text{at } \eta = i/N \text{ for } i = 1 \ldots N-1. \tag{24}$$

For stratified multilayer films of different fluids these conditions should be modified to include the viscosity and conductivity of each fluid giving the possibility of discontinuous velocity and temperature gradients between the layers. In our case the continuity of stress and heat flux give continuous velocity and temperature gradients as expected in the case of a single fluid layer.

We integrate the governing equations (4)-(6) and apply the surface and wall boundary conditions to first obtain the multi-layered model for arbitrary velocity and temperature profiles. To do this, the continuity equation (4) is integrated through the complete film depth which, with Leibnitz' rule, the surface kinematic condition (15) and the no-penetration condition (19) gives $\int_0^h u dy$ =constant. The constant represents the dimensionless volume flow rate per unit width and is found by integrating the far-field Nusselt

velocity profile (12). We split the integral of u over the complete film into its components from each layer to give

$$\int_0^h u dy = h\int_0^1 u d\eta = h\sum_{i=1}^{N}\int_{(i-1)/N}^{i/N} u_i d\eta = \int_0^h u_{\mathrm{NU}}(y)dy = 1. \tag{25}$$

The momentum (5) and energy (6) equations are integrated across each layer individually from $y = d_{i-1}$ to $y = d_i$. For brevity we introduce the notation $f|_i = f_i(\eta = \eta_i, x)$ to denote the value of a variable f at the upper boundary of layer i and $f|_{i-1} = f(\eta = \eta_{i-1}, x)$ its value at the lower boundary. To integrate the inertia term on the left-hand side of (5) we use Leibnitz' rule so to obtain

$$\int_{d_{i-1}}^{d_i}\left[\partial_x(u^2) + \partial_y(vu)\right]dy = \partial_x\int_{d_{i-1}}^{d_i} u_i^2 dy - u_i^2\big|_i\, d_i' + u_i^2\big|_{i-1}\, d_{i-1}' + (u_i v_i)|_i - (u_i v_i)|_{i-1}\,. \tag{26}$$

The slopes of the layer boundaries (d_{i-1}' and d_i') are related to the slope of the film height since $\eta = y/h$. Thus (26) is written in terms of η as

$$\partial_x\left(h\int_{\eta_{i-1}}^{\eta_i} u_i^2 d\eta\right) + (\,u_i\,(v_i - \eta h' u_i))|_i - (\,u_i\,(v_i - \eta h' u_i))|_{i-1}\,. \tag{27}$$

Taking the notation $[f]_{i-1}^i = f|_i - f|_{i-1}$, the second and third terms of (27) can be written as $[u_i(v_i - \eta h' u_i)]_{i-1}^i$. Integrating the heat convection term from (6) similarly we obtain the integral forms of the momentum and energy equations in each layer ($i = 1 \ldots N$):

$$\mathcal{M}_i \equiv R\left\{\partial_x\left(h\int_{\eta_{i-1}}^{\eta_i} u_i^2 d\eta\right) + \underbrace{[u_i(v_i - \eta h' u_i)]_{i-1}^i}_{(I)}\right\} + 3\epsilon\cot\alpha\frac{hh'}{N} - C\frac{hh'''}{N} - \frac{3h}{N} - \frac{1}{h}\left[\frac{\partial u_i}{\partial\eta}\right]_{i-1}^{i} = 0, \tag{28}$$

$$\mathcal{E}_i \equiv P\left\{\partial_x\left(h\int_{\eta_{i-1}}^{\eta_i} u_i T_i d\eta\right)\underbrace{+\,[T_i(v_i - \eta h' u_i)]_{i-1}^i}_{(II)}\right\} - \epsilon^2 h\int_{\eta_{i-1}}^{\eta_i}\frac{\partial^2 T_i}{\partial x^2}d\eta - \frac{1}{h}\left[\frac{\partial T_i}{\partial\eta}\right]_{i-1}^{i} = 0. \tag{29}$$

The terms labelled (I) and (II) in (28) and (29) represents the net flux of $x-$momentum and energy respectively into the i-th layer from the layers immediately above and below it; a positive value of this quantity indicates a net loss of momentum or energy from that layer. While we have not explicitly used the surface kinematic (15) and no-penetration

(19) boundary conditions in formulating (28)-(29), these are imposed when evaluating these equations in the top and bottom layers. In particular the upper limit of term (I) in the top layer ($i = N$) is zero by the kinematic condition (15), since the free surface is a material interface across which no mass transfers, and the lower limit of (I) in the bottom layer ($i = 1$) is zero by use of the no-penetration condition (19), since there is flow through the wall. Similarly for term (II) in the energy equation.

2.3. Polynomial velocity and temperature profiles

In each layer we approximate the $x-$velocity and temperature fields by quadratic polynomials in η with coefficients $a_{ij}(x)$ and $b_{ij}(x)$ $(j = 0 \dots 2)$ which depend on x:

$$u_i(x,\eta) = a_{i0}(x) + a_{i1}(x)\eta + a_{i2}(x)\eta^2 \quad \text{for } i = 1 \dots N, \tag{30}$$

$$T_i(x,\eta) = b_{i0}(x) + b_{i1}(x)\eta + b_{i2}(x)\eta^2 \quad \text{for } i = 1 \dots N. \tag{31}$$

Substitution of the profiles (30)-(31) into the surface shear stress boundary condition (16) gives an equation relating the velocity profile coefficients to the first derivative of the temperature profile coefficients in the top layer ($i = N$):

$$a_{N,1} + 2a_{N,2} = -Mh\left(b'_{N,0} + b'_{N,1} + b'_{N,2}\right) \equiv -m. \tag{32}$$

The surface heat transfer condition (17) provides a relationship between the temperature profile coefficients in the top layer:

$$Bihb_{N,0} + (1 + Bih)b_{N,1} + (2 + Bih)b_{N,2} = 0. \tag{33}$$

The wall boundary conditions of no-slip velocity (18) and fixed temperature (20) set the values of $a_{i,0}$ and $b_{i,0}$ in the first layer ($i = 1$):

$$a_{1,0} = 0, \tag{34}$$

$$b_{1,0} = T_w(x). \tag{35}$$

The matching conditions enforcing continuity of u and T between layers (21)-(22) provide the following set of algebraic equations:

$$a_{i,0} + a_{i,1}\left(\frac{i}{N}\right) + a_{i,2}\left(\frac{i}{N}\right)^2 = a_{i+1,0} + a_{i+1,1}\left(\frac{i}{N}\right) + a_{i+1,2}\left(\frac{i}{N}\right)^2 \qquad \text{for } i = 1 \dots N-1, \tag{36}$$

$$b_{i,0} + b_{i,1}\left(\frac{i}{N}\right) + b_{i,2}\left(\frac{i}{N}\right)^2 = b_{i+1,0} + b_{i+1,1}\left(\frac{i}{N}\right) + b_{i+1,2}\left(\frac{i}{N}\right)^2 \qquad \text{for } i = 1 \dots N-1. \tag{37}$$

The matching conditions on the stress tensor and heat flux (23)-(24) give

$$a_{i,1} + 2\left(\frac{i}{N}\right)a_{i,2} = a_{i+1,1} + 2\left(\frac{i}{N}\right)a_{i+1,2} \qquad \text{for } i = 1 \dots N-1, \tag{38}$$

$$b_{i,1} + 2\left(\frac{i}{N}\right)b_{i,2} = b_{i+1,1} + 2\left(\frac{i}{N}\right)b_{i+1,2} \qquad \text{for } i = 1 \dots N-1. \tag{39}$$

The layered model comprises $2N+1$ ordinary differential equations arising from a momentum (28) and energy (29) equation in each layer and the continuity equation (25) for the complete film. We choose as the corresponding $2N+1$ independent variables, the film profile h and the coefficient of the linear term in the velocity and temperature profiles in each layer, i.e. $a_{i,1}$ and $b_{i,1}$ ($i = 1 \dots N$). The final step of the formulation is to use the system of equations (32)-(39) to obtain all other coefficients from (30) and (31) in terms of these solution variables.

Though (32) is a differential equation, we treat it at this stage as an algebraic equation which relates $a_{N,1}$ and $a_{N,2}$ with a value of m known. This is because we will later obtain a relationship giving $b_{N,0}$ and $b_{N,2}$ in terms of $b_{N,1}$ which will be a solution variable so that, after discretization using a spectral collocation method (see Section 2.4), the right-hand side of (32) will become an algebraic expression which can be evaluated at each step of the iterative numerical solution procedure. Hence in our formulation we use (32) as an algebraic relation between $a_{N,1}$ and $a_{N,2}$. We now detail the steps whereby coefficients $a_{i,0}$, $a_{i,2}$, $b_{i,0}$ and $b_{i,2}$ for $i = 1 \dots N$ are obtained in terms of $a_{i,1}$ and $b_{i,1}$.

Coefficient $b_{1,0}$ is given directly by (35). From (37) and (39)

$$b_{i,0} = b_{i-1,0} + \frac{i-1}{2N}\left(b_{i-1,1} - b_{i,1}\right) \tag{40}$$

which is applied recursively from $i = 2 \dots N$. From (39)

$$b_{i,2} = b_{i+1,2} + \frac{N}{2i}\left(b_{i+1,1} - b_{i,1}\right), \tag{41}$$

which is applied recursively from $i = N-1$ to $i = 1$. The interface heat transfer condition (33) is rearranged to give

$$b_{N,2} = \frac{-1}{2+Bih}(Bihb_{N,0} + (1+Bih)b_{N,1}). \tag{42}$$

At this point all temperature profile coefficients in (31) are given in terms of $b_{i,1}$ and h. The velocity profile coefficients follow similarly. Coefficient $a_{1,0} = 0$ by (34). From (36) and (38)

$$a_{i,0} = a_{i-1,0} + \frac{i-1}{2N}\left(a_{i-1,1} - a_{i,1}\right) \tag{43}$$

which is applied recursively from $i = 2 \ldots N$. From (36)

$$a_{i,2} = a_{i+1,2} + \frac{N}{2i}(a_{i+1,1} - a_{i,1}), \tag{44}$$

which is applied recursively from $i = N-1$ to $i = 1$. With m known, the Marangoni surface shear condition (32) becomes an algebraic equation from which $a_{N,2}$ is obtained

$$a_{N,2} = \frac{-1}{2}(a_{N,1} + m). \tag{45}$$

It is worth noting at this stage that all boundary and matching conditions (15)-(24) have been used to solve the system in terms of variables h, $a_{i,1}$ and $b_{i,1}$. With all coefficients in (30) and (31) known in terms of these solution variables the integrated governing equations can be evaluated. The continuity equation for the complete film (25) becomes

$$\mathcal{C} \equiv h\sum_{i=1}^{N}\left\{\frac{a_{i,0}}{N} + \frac{a_{i,1}}{2N^2}(i^2-(i-1)^2) + \frac{a_{i,2}}{3N^3}(i^3-(i-1)^3)\right\} = 1. \tag{46}$$

The single nonlinear function $\mathcal{C}$, representing the the integrated continuity equation with parabolic forms for the velocity and temperature, depends on h and all other the coefficients in (30) and (31).

Substitution of (30) and (31) into the integrals on the left-hand sides of (28) and (29)

respectively give

$$\int_{(i-1)/N}^{i/N} u_i^2 d\eta = a_{i,1}^2 i/N^3 - a_{i,1}^2/3N^3 - a_{i,2}^2/5N^5 - a_{i,0}^2/N + a_{i,2}^2 i/N^5 - a_{i,1}^2 i^2/N^3 - 2a_{i,2}^2 i^2/N^5$$
$$+2a_{i,2}^2 i^3/N^5 - a_{i,2}^2 i^4/N^5 + a_{i,0}a_{i,1}/N^2 - 2a_{i,0}a_{i,2}/3N^3 + a_{i,1}a_{i,2}/2N^4$$
$$-2a_{i,0}a_{i,1}i/N^2 + 2a_{i,0}a_{i,2}i/N^3 - 2a_{i,1}a_{i,2}i/N^4 - 2a_{i,0}a_{i,2}i^2/N^3$$
$$+3a_{i,1}a_{i,2}i^2/N^4 - 2a_{i,1}a_{i,2}i^3/N^4 \tag{47}$$

and

$$\int_{(i-1)/N}^{i/N} u_i T_i d\eta = a_{i,0}b_{i,0}/N - a_{i,0}b_{i,1}/2N^2 - a_{i,1}b_{i,0}/2N^2 + a_{i,0}b_{i,2}/3N^3 + a_{i,1}b_{i,1}/3N^3$$
$$+a_{i,2}b_{i,0}/3N^3 - a_{i,1}b_{i,2}/4N^4 - a_{i,2}b_{i,1}/4N^4 + a_{i,2}b_{i,2}/5N^5 + a_{i,0}b_{i,1}i/N^2 + a_{i,1}b_{i,0}i/N^2$$
$$-a_{i,0}b_{i,2}i/N^3 - a_{i,1}b_{i,1}i/N^3 - a_{i,2}b_{i,0}i/N^3 + a_{i,1}b_{i,2}i/N^4$$
$$+a_{i,2}b_{i,1}i/N^4 - a_{i,2}b_{i,2}i/N^5 + a_{i,0}b_{i,2}i^2/N^3 + a_{i,1}b_{i,1}i^2/N^3$$
$$+a_{i,2}b_{i,0}i^2/N^3 - 3a_{i,1}b_{i,2}i^2/2N^4 - 3a_{i,2}b_{i,1}i^2/2N^4 + a_{i,1}b_{i,2}i^3/N^4$$
$$+a_{i,2}b_{i,1}i^3/N^4 + 2a_{i,2}b_{i,2}i^2/N^5 - 2a_{i,2}b_{i,2}i^3/N^5 + a_{i,2}b_{i,2}i^4/N^5. \tag{48}$$

Substitution of (30) into the integrated viscous term in (28), and of (31) into the integrated conduction term in (29) allow these to be written as

$$\left[\frac{\partial u_i}{\partial \eta}\right]_{(i-1)/N}^{i/N} = \frac{2a_{i,2}}{N}, \qquad \text{and} \qquad \left[\frac{\partial T_i}{\partial \eta}\right]_{(i-1)/N}^{i/N} = \frac{2b_{i,2}}{N}. \tag{49}$$

The x-conduction term from (29) is given as

$$\int_{(i-1)/N}^{i/N} \frac{\partial^2 T_i}{\partial x^2} d\eta = \frac{b''_{i,0}}{N} + \frac{b''_{i,1}}{2N^2}(i^2 - (i-1)^2) + \frac{b''_{i,2}}{3N^3}(i^3 - (i-1)^3). \tag{50}$$

The net inter-layer fluxes of $x-$momentum and energy, viz (I) in (28) and (II) in (29), require evaluation of the velocity and temperature fields at the inter-layer interfaces. For u and T these are calculated using (30) and (31) and give respectively

$$u_i|_i = a_{i,0} + \left(\frac{i}{N}\right) a_{i,1} + \left(\frac{i}{N}\right)^2 a_{i,2} \quad \text{and} \quad T_i|_i = b_{i,0} + \left(\frac{i}{N}\right) b_{i,1} + \left(\frac{i}{N}\right)^2 b_{i,2}. \tag{51}$$

Integration of the continuity equation (4) with respect to η gives v in layer i in terms of v on the upper surface of layer $i-1$ and an integral of u within the i-th layer:

$$v_i(\eta, x) = v_{i-1}|_{i-1} - h \int_{\eta_{i-1}}^{\eta} \frac{\partial u_i(\tilde{\eta}, x)}{\partial x} d\tilde{\eta}. \tag{52}$$

The integral in (52) is written in terms of the coefficients from (30) giving v on the upper surface of layer i as

$$v_i|_i = v_{i-1}|_{i-1} - h \left[\frac{a'_{j,0}}{N} + \frac{a'_{j,1}}{2N^2}(i^2 - (i-1)^2) + \frac{a'_{j,2}}{3N^3}(i^3 - (i-1)^3) \right], \tag{53}$$

which is applied recursively for $i = 1 \ldots N$ with the first step ($i = 1$) being the application of the no-penetration condition (19) $v_0 = 0$.

At this stage all terms in the integrated continuity, momentum and energy equations can be calculated in terms of h, $a_{j,1}$ and $b_{j,1}$ which for convenience we combine into a vector

$$\mathbf{x} = [h, a_{1,1}, \ldots, a_{N,1}, b_{1,1}, \ldots, b_{N,1}]^T. \tag{54}$$

The layered model can be expressed generally in the form of a non-linear vector function defined

$$\mathbf{F}(\mathbf{x}) = [C, \mathcal{M}_1, \ldots, \mathcal{M}_N, \mathcal{E}_1, \ldots, \mathcal{E}_N]^T. \tag{55}$$

$\mathbf{F}$ comprises the continuity equation $\mathcal{C}$ from (46), N momentum equations $\mathcal{M}_i$ from (28) and N energy equations $\mathcal{E}_i$ from (29). In general each C, $\mathcal{M}_i$ and $\mathcal{E}_i$ depend on all coefficients from all layers and generally the temperature and velocity fields are coupled. In the simpler case where $M = 0$ the film height is uniform, the velocity is given by the Nusselt profile and only the temperature field must be solved from (29).

2.4. Numerical solution of the model

The numerical solution of our model involves approximation of the derivative terms with pseudospectral differences. The infinite plane is truncated to $-L \leq x \leq L$ with L sufficiently large that the flow and temperature fields decay to the basic state (11)-(14) at the upstream and downstream ends of the domain within numerical accuracy so that periodic conditions can be applied at there. We introduce a computational domain ξ which is related to the physical domain x by $x = f(\xi)$. f is chosen in such a way that grid

points are clustered closely near the heated section and distributed sparsely elsewhere. This saves on computational expense since most of the deviation from the basic Nusselt flow takes place within a short distance of the heater. We choose the transformation

$$f(\xi) = L\frac{\sinh(c\xi/\pi)}{\sinh c}. \tag{56}$$

The parameter c controls the non-uniformity where $c = 1$ corresponds to a uniform physical grid and $c > 1$ clusters the mesh points around the heater. The computational mesh covers $-\pi < \xi \leq \pi$ using K grid points equally spaced at $\xi = \xi_k = \pi(2k/K - 1)$ for $k = 1 \ldots K$ with no point at $\xi = -\pi$ due to the periodic condition. Derivatives on the computational domain are evaluated using Fourier collocation differentiation matrices and derivatives on the physical domain are related to these using the transformations

$$\frac{d}{dx} = \frac{1}{f'}\frac{d}{d\xi}, \tag{57}$$

$$\frac{d^2}{dx^2} = \frac{1}{(f')^3}\left[f'\frac{d^2}{d\xi^2} - f''\frac{d}{d\xi}\right], \tag{58}$$

$$\frac{d^3}{dx^3} = \frac{1}{(f')^5}\left[(f')^2\frac{d^3}{d\xi^3} - 3f'f''\frac{d^2}{d\xi^2} + (3(f'')^2 - f'f''')\frac{d}{d\xi}\right]. \tag{59}$$

Discretizing the ODE system (55) yields $(2N + 1)K$ coupled, nonlinear, algebraic equations which are solved numerically using the Matlab function `fsolve`. This uses the Newton-Raphson method to approximate $\mathbf{x}$. The Jacobian of the system is approximated at each step using finite differences. At each iteration we also approximate m using spectral collocation so we are able to use (32) as an algebraic equation relating $a_{N,1}$ and $a_{N,2}$.

From the approximate solution the remaining coefficients in (30) and (31) are calculated. The effect of the domain truncation on each solution is quantified by calculating the residual

$$\text{res} = \max_{i=1\ldots N}\{|h - 1|, |a_{i,1} - 3|, |b_{i,1}|\} \text{ at } x = L, \tag{60}$$

which measures how closely the numerical solution matches the the Nusselt solution in the far field. Note from comparison of the quadratic profiles (30) and (31) with the Nusselt solution (12) and (14) the layered model should give $a_{i,1} = 3$ and $b_{i,1} = 0$ in the far field. All results shown in this paper have res $< 10^{-5}$.

3. Numerical solution with negligible Marangoni effects

In this section we consider films neglecting Marangoni effects and compare results from the multi-layer IBL model to those from a full numerical solution of the two-dimensional energy equation (6) using finite differences. In this case the film height is uniformly, $h = 1$, and the Nusselt velocity profile (12) persists throughout the film. The film temperature is given from solving the energy equation (6) which simplifies to

$$3P\left(y - \tfrac{1}{2}y^2\right)\frac{\partial T}{\partial x} = \epsilon^2\frac{\partial^2 T}{\partial x^2} + \frac{\partial^2 T}{\partial y^2}, \tag{61}$$

within the fixed domain $-\infty < x < \infty$, $0 \le y \le 1$. Boundary conditions (20) and (9) are applied to (61). Equation (61) is solved using second-order accurate finite differences on a uniform mesh which is truncated in the x-direction which is chosen to be sufficiently long that the temperature has decayed to below 10^{-5} everywhere along these boundaries. Far-field conditions are applied directly (i.e. they are not replaced by periodic conditions) and the algebraic system is solved using the Matlab function `fsolve` and the following wall temperature profile

$$T_w(x) = e^{-\frac{1}{2}x^2}. \tag{62}$$

(This profile is used for all results in this paper except for those at the end of Section 4 where we use a different exponential profile to compare with results published in [18]). Results in figure 2 show a comparison between temperature fields predicted using the layered model with $N = 1, 2, 4, 8$ and the two-dimensional finite-difference solution of (61). A value of $P = 10$ was used corresponding to strong convection resulting in the locally heated region being driven downstream. The temperature field obtained using a single layer exposes the main inaccuracy of the IBL model, namely the region of negative temperature near the surface immediately upstream of the heater (shown hatched in the figure). The minimum film temperature in this region is -3×10^{-2}. This phenomenon has been observed in [20]. The advantage of the multi-layer model is clear for $N = 2$ as this region is markedly reduced and the minimum temperature is -0.002047. For $N = 4$ and 8 the region is negligible and minimum temperatures of the order -1×10^{-8}. The L_2-error norm of the layered model solution compared to the 2DFD solution (denoted T_{2DFD}) within the heated region is given as

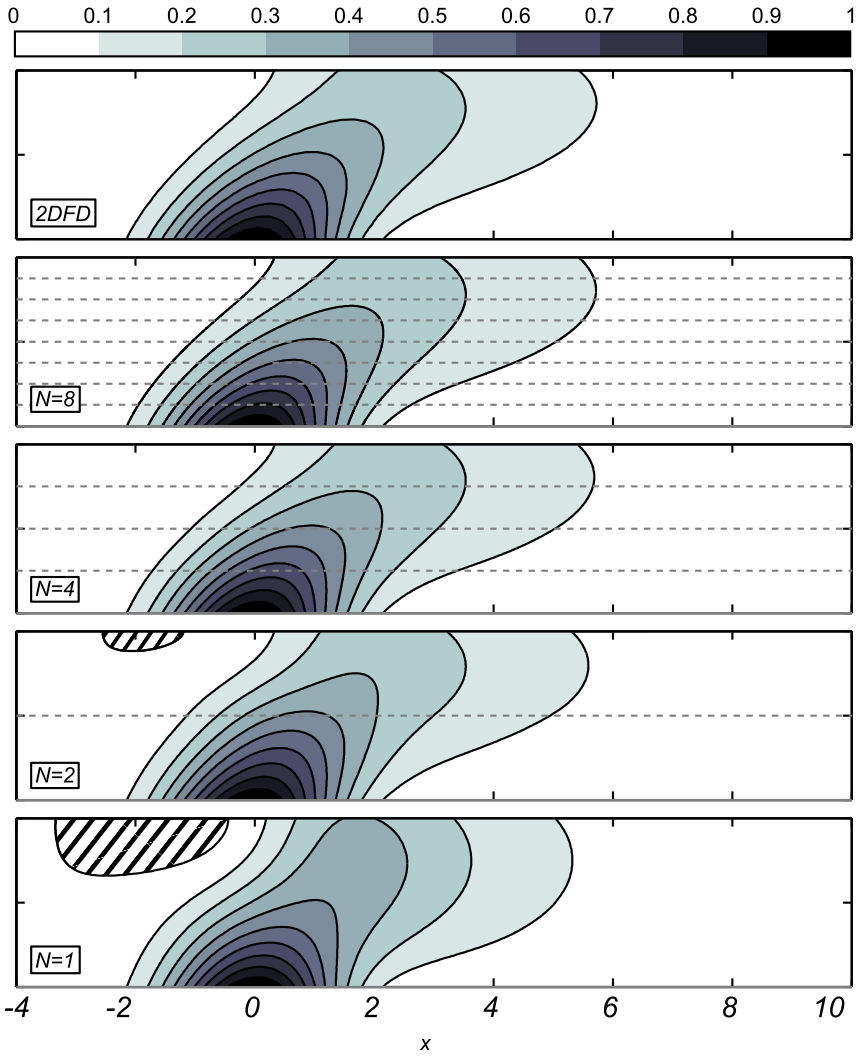

Figure 2: Calculated temperature fields in a uniform film over a heated region using 2DFD and layered model. Hatched region indicates negative temperature. $\epsilon = 0.1$, $P = 10$, $Bi = 1$, $M = 0$.

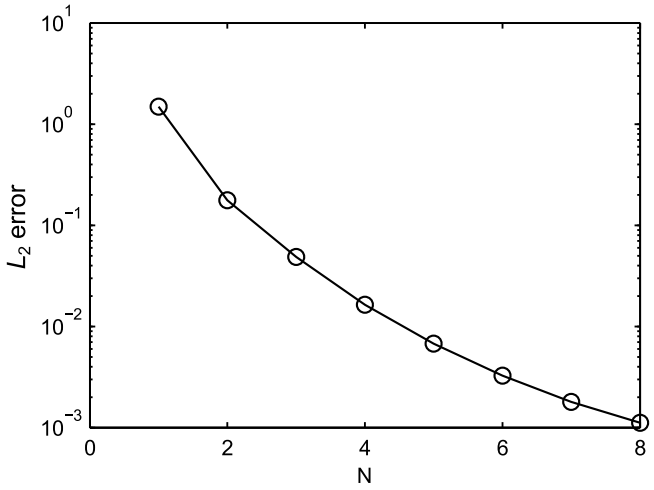

Figure 3: L_2 error norm (63) of layered model solutions for temperature fields in figure 2. $\epsilon = 0.1$, $P = 10$, $Bi = 1$, $M = 0$.

$$L_2 \text{ error} = \int_0^1 \int_{-5}^{10} \left[T(x,y) - T_{2DFD}(x,y)\right]^2 dxdy. \tag{63}$$

This is plotted in figure 3. This confirms that the temperature field converges with increasing N and the error is seen to reduce by three orders of magnitude between $N = 1$ and 8.

The inherent problem with using a quadratic polynomial to approximate the film temperature using a single layer is that it does not provide the flexibility required to model complex temperature distributions. This can be manifest by unphysical solutions; temperature profiles through the films in figure 2 are shown in the left panel of figure 4 where the region of negative temperature can clearly be identified. In this case two of the three coefficients in the quadratic temperature profile are defined by the surface and wall boundary conditions leaving the third to be determined by imposing that the complete profile should satisfy the integrated energy equation across the complete film. The latter constraint necessitates the introduction of the negative temperature region to balance the temperature overestimation in the lower half of the film and allow the energy equation to be satisfied in an average sense. In the right panel of figure 4 the temperature profiles at $x = 1.3$ are shown. Here the inaccuracy of the single profile is

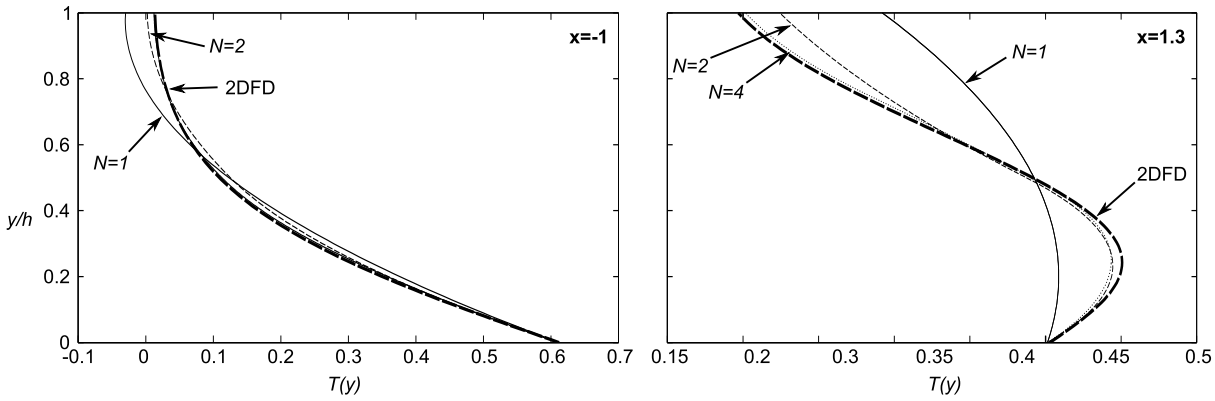

Figure 4: Profiles of temperature through film depth at $x = -1$ (left) and $x = 1.3$ (right) for layered and 2DFD solutions. $\epsilon = 0.1$, $P = 10$, $Bi = 1$, $M = 0$.

more significant though does not give rise to a negative temperature. The exact 2DFD solution is clearly not quadratic and, though the single layer solution satisfies both the wall and surface conditions it is unable to model the temperature distribution close to the wall giving a poor estimation of both maximum and surface temperatures. With two layers the integrated energy equations must be satisfied in an average sense across only half of the film thickness each. This allows the upper and lower boundary conditions to be satisfied with more flexibility to represent the local flow conditions in each layer. The improvement is clearly seen as the profiles through the film at both $x = -1$ and $x = 1.3$ for $N = 2$ replicate the features of the 2DFD solution considerably better. It was found that with three layers the profile at $x = -1$ was indistinguishable from the 2DFD solution. At $x = -1.3$ the four-layered profile shows a small discrepancy in the lower half of the film where the maximal film temperature is underestimated, it was found that for $N = 8$ profiles are indistinguishable.

We also performed the same analysis for $P = 0.1$ and 1 corresponding to weak convection. In both cases the IBL model gave excellent agreement with the 2DFD solution including for $N = 1$. This is expected as the exact solution to the temperature field for a conduction-dominated film is linear in y and so can be exactly represented by a quadratic polynomial.

4. Film profiles with Marangoni effects

When Marangoni effects are included the film profile is generally non-uniform as any local heating creates a surface tension gradient which in turn drives a surface shear stress via the boundary condition (8). This stress moves fluid against any surface temperature gradient creating a standing wave over the heated region. This effect has been studied widely using models based on lubrication theory and with IBL models using a single layer such as [18]. In this section we analyse how use of the multi-layer model affects the film profile and temperature field.

Film height profiles and temperature fields for two cases of flow, a conduction-dominant film with $R = 1$, $P = 1$ and a convection-dominant film with $R = 5$, $P = 5$ are considered and illustrated in figure 5. We choose to consider a vertical plane ($\alpha = \pi/2$) as we do for all cases considered in this paper. With $R = 1$, $P = 1$ there is very little difference in solution as N is increased since the exact temperature dependence in y is linear. However for larger P and R the film height predicted with one layer differs significantly from that using the multi-layer model; there is a clear convergence of the solutions toward a common profile as the results are indistinguishable for $N > 2$. Physically, the reduction in maximum film height between the two cases of weak and strong convection is due to the reduced Marangoni stress in the convection-dominant film as more heat is driven downstream and gradually diffuses through the boundary. For $R = 1, P = 1$ the temperature gradient at the surface is larger and induces a higher stress.

Results highlight the importance of the multi-layered model for convection-dominant flows when the temperature through the film differs from linear. Further evaluation reveals that the difference in film height from $N = 1$ to 2 is due to the improved prediction of surface temperature which is plotted in figure 6(a) for $N = 1, 2, 3$. For $N = 1$ there is a negative temperature (minimum $T = -2.6 \times 10^{-2}$) close to $x = -2$ (location labelled in figure 5) which is reduced to -10^{-6} for $N = 2$. An erroneous negative surface temperature leads to an error in Marangoni stress from (8) and an inaccurate film height. For $N = 2$ the Marangoni stress and hence film height are more accurate. Temperature profiles through the film at $x = -2$ are also plotted which show the reduction in the unphysical temperature region for $N \geq 2$.

Figure 7 shows comparison profiles of $u(y) - u_{\mathrm{NU}}(y)$ through the depth of the film

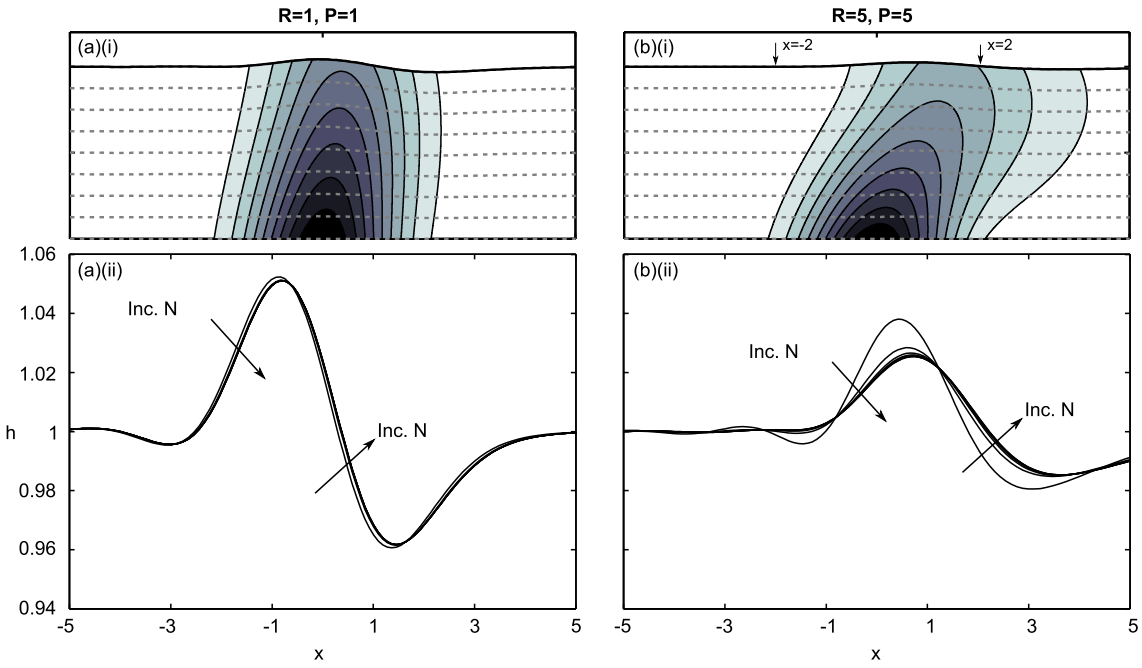

Figure 5: Effect of N on the film temperature (i) and film height profile (ii) for conduction- and convection-dominant flows with $N = 1 \ldots 8$. In (a) $R = 1$, $P = 1$, in (b) $R = 5$, $P = 5$. For both $\epsilon = 0.1$, $Bi = 1$, $M = 1$, $C = 1$, $\alpha = \pi/2$. Colormap in (i) shows 10 equally spaced temperature intervals from 0 (white) to 1 (black). Arrows in (b)(ii) indicate locations of profiles plotted in figures 6 and 7.

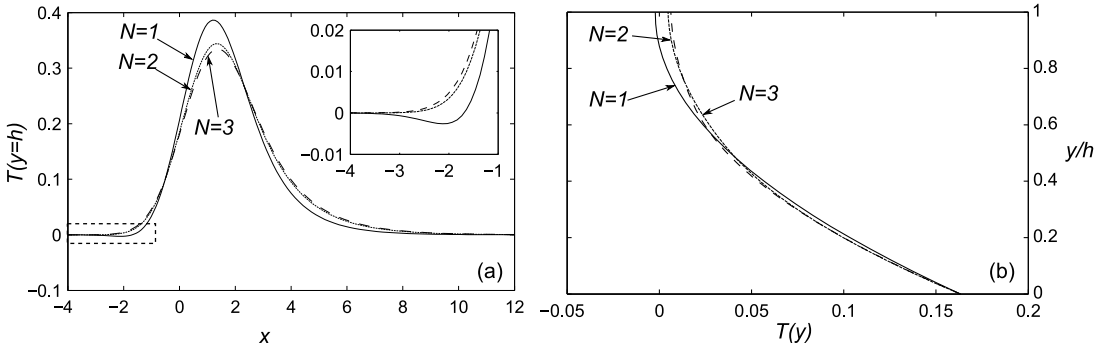

Figure 6: Effect of number of layers. (a) film surface temperature with inset showing detail and (b) temperature profiles through the film thickness at $x = -2$ (position marked in figure 5). $\epsilon = 0.1$, $R = 5$, $P = 5$, $Bi = 1$, $M = 1$, $C = 1$, $\alpha = \pi/2$.

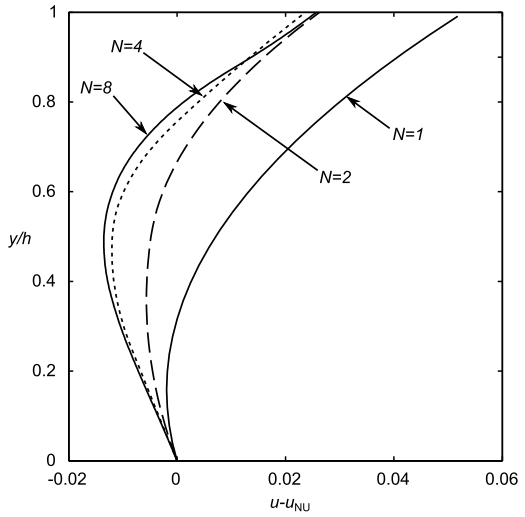

Figure 7: Effect of N on the velocity profile $u(y) - u_{\mathrm{NU}}(y)$ at $x = 2$ (position marked in figure 5). $\epsilon = 0.1$, $R = 5$, $P = 5$, $Bi = 1$, $M = 1$, $C = 1$, $\alpha = \pi/2$.

at $x = 2$ (as indicated by an arrow in figure 5(bii). The film profile changes significantly with N. Since $u_N(y)$ is the quadratic Nusselt velocity profile valid far from the heater this plot effectively isolates the effect of the Marangoni surface stress on the velocity field. The inadequacy of a quadratic velocity profile for a single layer is clear as the profile is significantly different than for $N \geq 2$. Temperature profile in velocity across the film depth improves with N as each averaged energy equation does not need to be satisfied over such a large portion of the film depth. A small inflection in the velocity profile very close to the surface (around $y/h = 0.9$) emerges for $N = 8$. This localized feature cannot could not be effectively modelled without the flexibility of multiple layers.

A convergence analysis is performed on the solutions for $N = 1 \ldots 8$ by considering the variation in maximum film height with number of layers. The quantity

$$C_j = \frac{c_j - c_8}{c_8} \tag{64}$$

is considered where c_j is the maximum film height using j layers. A plot of how c_j this varies as R and P each take values 0.1, 1 and 5 is shown in figure 8. For all cases the quantity converges as N increases indicating that increasing the number of layers improves accuracy. For cases of low P and R there is a negligible change in the

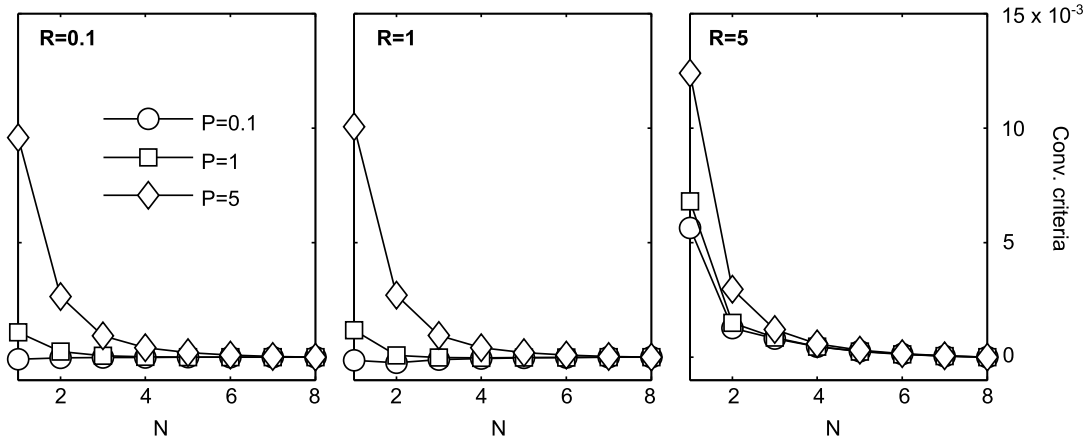

Figure 8: Convergence analysis for film height. $\epsilon = 0.1$, $Bi = 1$, $M = 1$, $C = 1$, $\alpha = \pi/2$.

maximum film height with N; when either R or P are large, more layers are needed (larger N) to obtain the same accuracy.

An important feature of our layered model is the inclusion of inertia in the momentum equation. Here we show how this modifies the film profiles shown in figure 5(a)(ii) by fixing $P = 1$ and changing R so to isolate on the inertial effects. Profiles are shown in figure 9 for $R = 0.1$, 1, 3 and 5. As with previous studies into the effect of inertia on steady standing-waves [32] we find that increasing R moves the feature downstream and has a smoothing effect in the region of the disturbance. The width of the disturbance also increases with R so that for cases of $R > 5$ the decay in amplitude of the waves takes place over such a long distance that it is difficult to obtain, with a modest number of grid points, an accurate solution which has sufficiently decayed at the ends of the computational domain. To this end we only show results for up to $R = 5$. Equivalent film height profiles for $P = 5$ (not shown), are found to exhibit the same trend however the amplitude of the wave is reduced due to the reduction in surface gradient temperature, and hence Marangoni effect, brought about by the smoothing effect of convection.

To conclude this section we present a comparison of results from our layered model with those from the model presented in [18] which we henceforth term the KKH (Kalliadasis, Kiyashko and Demekhin) model. This model is based on a single-layer IBL approach with quadratic velocity profile and linear temperature profile and was used to

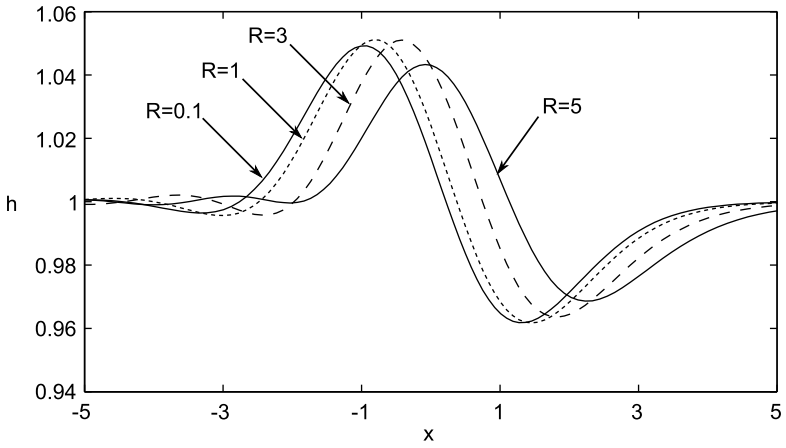

Figure 9: Effect of inertia on film height profiles. $\epsilon = 0.1$, $P = 1$, $Bi = 1$, $M = 1$, $C = 1$, $\alpha = \pi/2$, $N = 8$.

predict the stability locally-heated thin film flows. Here the basic steady state solution for the stability analysis is provided by a momentum equation which balances surface tension, hydrostatic pressure, the Marangoni stress and viscosity, and an energy equation which balances convection with conduction in the direction normal to the plane. Despite the IBL approach used to formulate the KKH model, inertial effects do not appear in the basic state of the KKH model (though they do in the stability analysis). Thus their steady-state momentum equation, against which we compare our model, is equivalent to that obtained using a lubrication theory approximation. Their steady-state energy equation includes heat convection effects, which would not be the case if using a lubrication theory alone.

To achieve an equivalent representation using our layered model requires setting $R = 0$ in (28) so removing inertial effects. In the KKH model, the down-plane distance is scaled with h_0 whereas in our model we scale with l so the aspect ratio in our model is $\epsilon = 1$ to achieve comparable results. Comparing (28) and (29) with their equivalents (17a) (momentum equation) and (17b) (heat equation) from [18] we see that $C = \epsilon^3 ReWe$ for $We = \sigma_0/\rho h_0 \hat{U}_0^2$ the film Weber number - used as the surface tension parameter in the KKH model. Similarly $P = \epsilon Pe = \epsilon RePr$. Finally we set the coefficient of $x-$conduction term in (29), which is given as ϵ^2 in our model, to a small parameter, here taken as 0.01, so to introduce a smoothing effect equivalent to that described in [18] where a term

proportional to a small multiple of d^2T_s/dx^2 was included to aid numerical solution.

We use the results of figures 2 and 3 of [18] to compare the KKH model to our layered model. These figures show steady-state profiles of film height h and film surface temperature $T_s = T(x, h)$ for a film falling on a vertical substrate ($\theta = \pi/2$) having temperature profile $T_w = \exp(-0.005x^2)$ with $Re = 1$, $Bi = 1$, $We = 4110$, $Pr = \nu/\kappa = 7$ at three values of the Marangoni number $Ma = 6$, 16 and 26. We solve our layered model for the equivalent set of parameters $\epsilon = 1$, $R = 0$, $P = 7$, $Bi = 1$, $C = 4110$, $\alpha = \pi/2$ and compare the film height and surface temperature profiles to those obtained from a numerical solution of equations (17a) and (17b) from [18]. We obtained these numerical solutions of the KKH model ourselves using Matlab's finite difference boundary value problem solver `bvp4c`. We follow the initialization procedure for this solver as outlined in [18] which corresponds to solving their steady heat equation with $Ma = 0$ to obtain an approximate surface temperature distribution for a flat film. An approximate film height profile is obtained from a linearized version of their steady momentum equation. Finally these are used to initialize the `bvp4c` solver.

Results from this comparison are shown in figure 10 where we have solved our layered model with one layer ($N = 1$) for consistency with the single layer of the KKH model. As can be expected, increasing M makes a larger peak and trough in film height above the heater since it causes increases the size of the surface shear in (16). The film height profiles obtained using the two models (left-hand panel of (a)) are almost identical at each value of M indicating that the two models are in excellent agreement. Similarly the surface temperature profiles in (b) predicted by the two models are almost indistinguishable. (We found that changing M had almost no effect on these profiles and so only plotted the case $M = 6$ for clarity).

The good agreement in film height profiles is because, in the absence of inertial effects ($R = 0$), the exact velocity profile through the film is quadratic in y as predicted using a lubrication theory. Since both the KKH model and our layered model are built using a quadratic velocity profile we can obtained this profile exactly. Nevertheless we cannot expect to obtain the exact temperature distribution since we include heat convection ($P = 7$). (Had $P = 0$ the film temperature profile would be a linear function in y.) However in this case, where the wall temperature and film height both vary slowly with

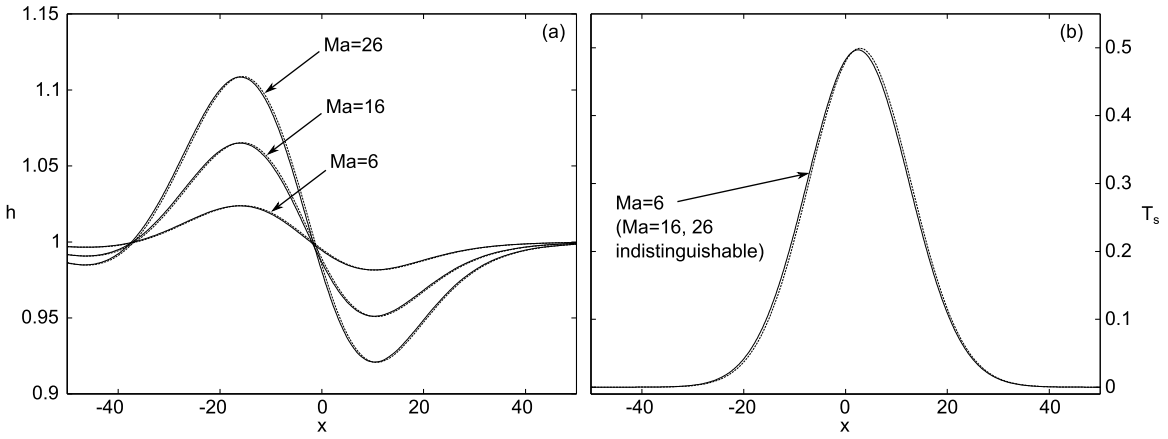

Figure 10: Comparison of results using the layered model (solid line) to that of [18] (dashed line). (a) Film height profiles, (b) surface temperature profiles. Parameters are $\epsilon = 1$, $R = 0$, $P = 7$, $C = 4110$, $Bi = 1$, $T_w(x) = \exp(-0.005x^2)$, $N = 1$.

x, all derivatives in the convection term are small so it has little effect on the solution - as confirmed by almost-identical temperature profiles in (b). We also solved the layered model for $N = 2 \ldots 8$ and found identical results, indicating that in this case, where the film height and temperature are slowly-varying with x, a single layer is sufficient to obtain very accurate results. This should be compared with results in figure 5 and 6 where a film with similar Péclet number ($P = 5$) but sharply varying wall temperature required more layers to obtain accurate resolution of the film profile and temperature field.

An important feature of our layered model is the inclusion of inertial terms in the momentum equation (28) which distinguishes it from the KKH model where inertial effects are only considered for their effect on the stability of the flow, not on the steady-state solution. For the results shown in figure 10 we find there is a negligible difference in film height profile if the inertial effects are included by setting $R = \epsilon Re = 1$. Despite this moderate value of R for these cases, inertia remains weak because stream-wise gradients in the inertial terms in (28) are small. This happens because the wall temperature profile decays very slowly with x so film height features which are driven by the associated Marangoni effect also vary slowly with x - compare the width of the waves in figure 10(a) with those in figure 9. Should the wall temperature profile be more localized, as it is in

figure 9, then inertial effects are significant and their inclusion modifies the film profile noticeably.

5. Numerical investigation

The model has twelve dimensional parameters (seven dimensionless) making the parameter space too large to investigate thoroughly. To progress we investigate solutions for a fixed working fluid (water) and heater and plane geometries. We change only the far-field film height h_0 and heater temperature $\Delta\hat{T}$. Physical values used for the tests are: $\rho = 997.05$ kg/m^3, $c = 4182$ J/kgK, $k = 0.6075$ W/mK, $\sigma_0 = 0.0728$ N/m, $\sigma_T = 0.00016$ N/mK, $\nu = 0.893\times10^{-6}$ m^2/s, $g = 9.81$ m/s^2, $L = 1$ mm and $\hat{T}_\infty = 20$ °C. The fluid properties have been obtained from [33]. As has been noted in previous studies [18, 34] it is difficult to determine the heat transfer coefficient of the film surface and so we fix a representative value at $\Gamma = 1000\,\mathrm{W/m^2K}$. A vertical plane is considered: $\alpha = \pi/2$.

h_0 [mm]	0.02	0.05	0.06	0.08	0.1	0.15	0.2
U_0 [mm/s]	1	9	13	23	37	82	146
ϵ	0.02	0.05	0.06	0.08	0.1	0.15	0.20
R	7×10^{-4}	0.026	0.053	0.17	0.4	2.1	6.6
P	4×10^{-3}	0.16	0.33	1.0	2.5	12.7	40.2
M	25	9.8	8.2	6.1	4.9	3.3	2.5
C	0.4	1.1	1.3	1.8	2.2	3.3	4.5
Bi	0.03	0.08	0.10	0.13	0.16	0.25	0.33

Table 1: Dimensionless parameters for the numerical experiment shown in figure 11. $\alpha = \pi/2$.

In the first study we fix $\Delta\hat{T} = 10$°C and consider varying far-field film heights h_0 between 0.02 and 0.2 mm. This gives the dimensionless parameters shown in table 1 where the mean velocities U_0 are obtained using (2). Temperature fields and streamlines for these flows are shown in figure 11 for $N = 8$. The results illustrate how the balance between heat convection and the Marangoni effect changes as the film thickness increases.

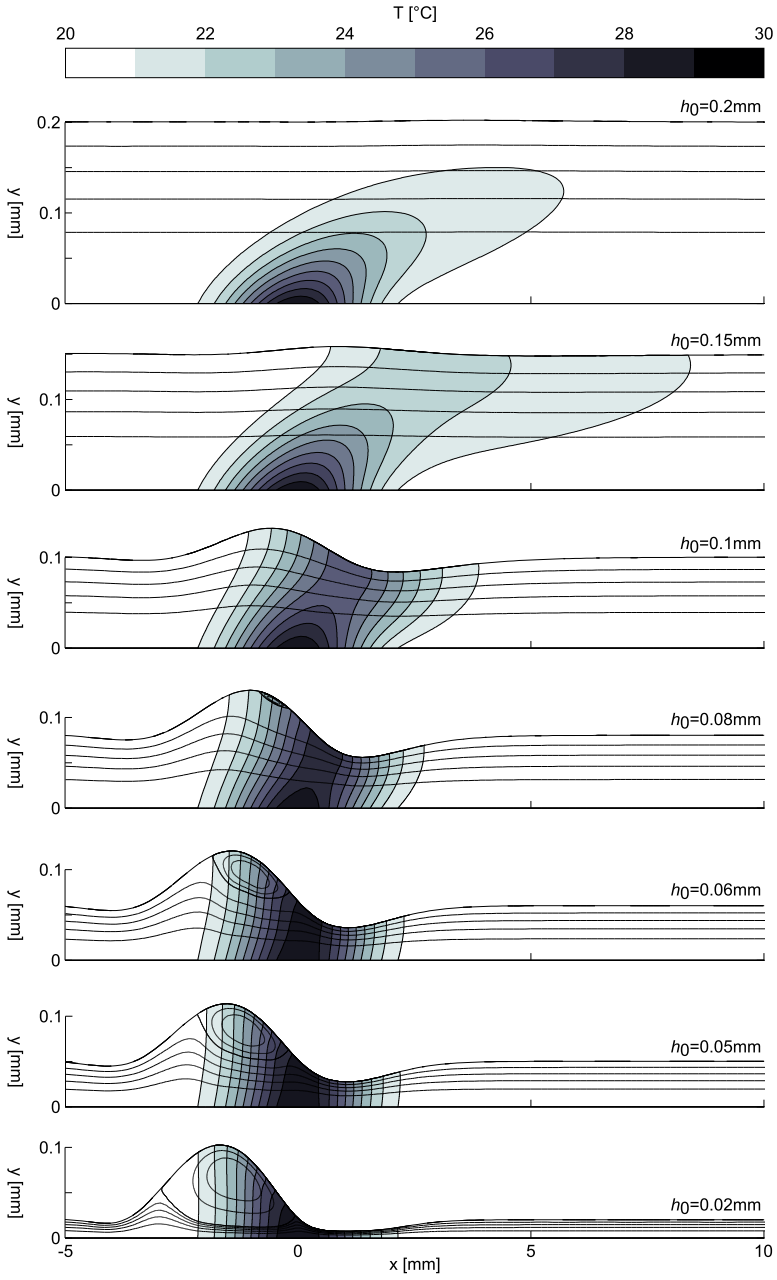

Figure 11: Film temperature fields and streamlines for different h_0. Parameters given in table 1.

For the thinnest film ($h_0 = 0.02$ mm) the temperature field displays negligible convection the wall temperature profile persists through the film depth from the wall to the surface. As such, the surface temperature gradient is large which induces shear stress which is sufficient to overcome gravity and form a recirculating eddy upstream of the heater near the film surface. For thicker films ($h_0 = 0.05 - 0.08$ mm) convective effects are stronger and more heat is transported downstream. Additionally the surface is more remote from the heating at the wall. Both these factors have the effect of reducing the surface temperature gradient and, as a consequence, the Marangoni effect is weaker. Thus the recirculation becomes smaller - at $h_0 = 0.08$ mm only a very small eddy is observed - and the film height profile becomes increasingly uniform. At $h_0 = 0.1$ mm the recirculation is removed and the flow is unidirectional. For $h_0 = 0.15$ mm the film thickness is almost uniform and at $h_0 = 0.2$ mm the heating effect is confined almost entirely within the film yielding a very small surface temperature gradient and hence an approximately-uniform film. In this case the velocity field and film profile are very close to the Nusselt solution (1) throughout.

A second study considers how the film is affected by the strength of heating. Results are shown in figure 12. We take the profile with $h_0 = 0.08$ mm from figure 11 which exhibits a small recirculation when $\Delta T = 10°\text{C}$ and increase the heater temperature to $\Delta\hat{T} = 12°\text{C}$. This temperature rise causes the recirculation to increasing in size and the peak in film height also increases due to the increased surface temperature gradient. The flow is very sensitive to the effects of $\Delta\hat{T}$ so that to obtain the results we have used a basic continuation method where $\Delta\hat{T}$ is increased in increments of 0.25 °C using the previous solution as an initial field for the numerical solver. Even so, it is still difficult to obtain accurate solutions (measured by the the residual in the Newton iterations) for $\Delta\hat{T} > 12°\text{C}$.

The recirculation region for $\Delta\hat{T} = 13°\text{C}$ is illustrated in figure 13 where it can be seen that its shape changes to become increasingly asymmetric. This necessitates increasing the resolution of points in the $x-$grid as well as including sufficient layers to resolve the complicated velocity profile in the $y-$direction. Combined, these demand an excessive amount of computation given that we must include both a momentum and energy equation simultaneously in each layer

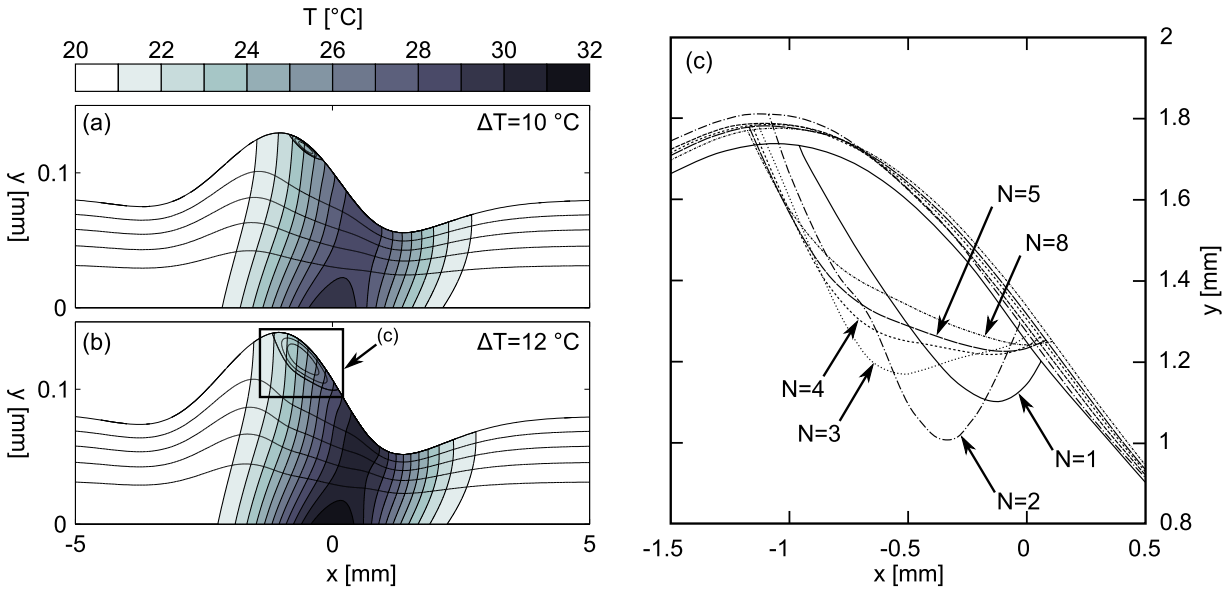

Figure 12: Temperature field and streamlines in film with $h_0 = 0.08$mm using 8 layers for $\Delta\hat{T} = 10°$C (a) and $12°C$ (b). (c) Film height and dividing streamline for $\Delta\hat{T} = 12°$C with $N = 1$, 2, 3, 4, 5 and 8.

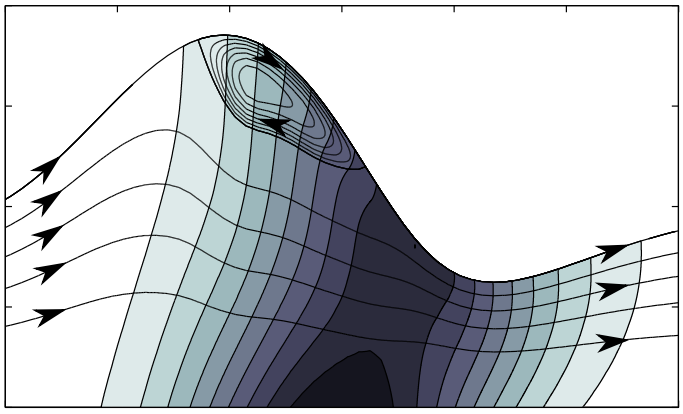

Figure 13: Temperature field and streamlines for film with $h_0 = 0.08$mm using 8 layers for $\Delta\hat{T} = 13°$C. Colourmap illustrates the temperature field using an equally spaced scale of ten shades from 0°C (white) to 13°C (black)

The sensitivity of these results to the number of layers was also tested by obtaining the $\Delta\hat{T} = 12°\mathrm{C}$ results for $N = 1 \ldots 8$. Figure 12 shows the film height profiles and dividing streamline around the recirculation for $N = 1$, 2, 3, 4, 5 and 8 (intermediate results not shown for clarity). There is clear convergence of the dividing streamline towards that with $N = 8$ and inaccuracies in the profile for low N manifest by an overestimation of the size of the recirculation.

6. Conclusion

Motivated by extensions in modelling capability which are brought about when a multi-layer approach is applied to shallow-water environmental flows, we have applied the approach to thin liquid film flowing over a locally-heated inclined plane. The liquid surface tension varies with temperature so that local heating can induce a surface temperature gradient, which in turn drives a surface shear stress and results in a non-uniform film height profile.

Typically in single-layer models the flow and temperature are taken to vary quadratically on distance from the plane. In this paper we extend this concept and split the film into a number of layers, each having a momentum and energy equation integrated across its thickness and the continuity equation for the film is integrated across the complete film. We apply matching conditions to the profiles between layers to ensure continuity requirements on the flow and to couple the equations from each layer together. The final model is solved numerically using a spectral collocation method to obtain the film height profile and a coefficient from the velocity and temperature profile in each layer. From these the remaining profile coefficients can be recovered and the film flow and temperature field calculated. Application of this new approach is undertaken to calculate thin film flows subject to Marangoni effects.

In the absence of Marangoni effects there is no surface shear stress and the film height is uniform, the velocity is given by the Nusselt solution (12) and only the temperature field must be sought numerically. In this case we solve the full heat equation using finite differences and compare the results with those from the multi-layer model. For cases of weak heat convection, both solutions are almost identical, even when the multi-layer model is used with only a single layer. For stronger convection, there appears a region of

negative (unphysical) temperature using a single layer. As further layers are added this is reduced and with four layers it is completely removed. A convergence test comparing the layered model against the finite difference solution of the full heat equation shows that, for in a film with strong convection, the numerical L_2 error norm of the multi-layer solution decreases by three orders of magnitude as the number of layers is increased from one to eight. It is observed that when convection is strong the variation in film temperature through the film depth can be complex and is not well approximated by a single quadratic profile across the complete film. While such a low-order profile for the complete film does satisfy the surface and wall boundary conditions and the integrated energy equation, the latter is achieved by the introduction of regions of negative temperature in order to remain satisfied on average across the complete film. As additional layers are added, the width of the region over which each integrated energy equation must be satisfied reduces and a low-order polynomial produces very accurate results.

When Marangoni effects are included the film height profile varies due to gradients in surface temperature arising local heating at the plane wall. A peak in film height appears at the upstream-side of the heated region as the surface stress there acts against the down-plane component of gravity causing a build-up of fluid. At the downstream-edge the Marangoni stress acts with gravity to accelerate the film leading to a trough. For weak convection, the temperature of the heater diffuses upwards to the surface leading to a high surface temperature gradient and hence this peak and trough configuration is pronounced. If convection is strong then a significant amount of heat is transferred downstream which lessens the temperature gradient on the film surface. This reduces the surface shear stress and the film is smoothed with the peak and trough becoming less pronounced. The weak-convection cases are well-modelled with a single layer since the exact solution to the temperature field in this case is a linear function y. If convection is strong then the exact solution is no-longer linear and extra layers are required to give an accurate solution. A convergence test shows the peak in film height converges as the number of layers are increased.

The effect of increasing the Reynolds number of the film is to reduce the height of disturbance in the heated region and to drive it downstream. This produces a significant change in film profile when the local temperature gradient on the wall is large however

if the wall temperature only varies gradually along the plane then even at a moderate Reynolds number there is little effect from inertia. The same is found for convective effects which are also driven by streamwise gradients in the flow and wall temperature.

Finally, a numerical experiment is performed using water on a vertical plane. Films are examined for a range of upstream film heights under a fixed heater temperature. For thin films the effect of the heater is significant and the dominant effects are heat conduction from the wall to the surface and the Marangoni stress which this induces. Consequently the film height varies significantly and the flow includes, for the thinnest films, a recirculation region brought about by the strong surface shear which is directed upstream against the flow at the upper-edge of the heater. For thicker films this feature reduces as the heating is further from the surface and more heat is conveyed downstream. Beyond a critical thickness the flow is completely unidirectional and for the thickest films the heating effect is confined completely within the film leading to a constant surface temperature and hence an undisturbed film height. In these cases the Marangoni effects is negligible, the flow given by the Nusselt profile and only the temperature field need be sought numerically. For a given film height, the recirculation can be formed by increasing the strength of heating and hence increasing the Marangoni number M. The number of layers used affects the size of the predicted recirculation region and its shape converges towards a fixed outline as the number of layers is increased.

We also compare our layered model a similar single-layer IBL model studied by [18] and found excellent agreement in results for the parameter ranges considered.

References

[1] A. Oron, S. H. Davis, S. G. Bankoff, Long-scale evolution of thin liquid films, Reviews of Modern Physics 69 (3) (1997) 931–980.

[2] R. V. Craster, O. K. Matar, Dynamics and stability of thin liquid films, Reviews of Modern Physics 81 (2009) 1131–1198.

[3] J. Weinstein, S, K. J. Ruschak, Coating Flows, Annual Review Fluid Mechanics 36 (2004) 29–53.

[4] C.-S. Yih, Instability due to viscosity stratification, Journal of Fluid Mechanics 27 (1967) 337–352.

[5] T. B. Benjamin, Wave formation in laminar flow down an inclined plane, Journal of Fluid Mechanics 2 (1957) 554–573. doi:10.1017/S0022112057000373.

[6] B. S. Tilley, S. H. Davis, S. G. Bankoff, Linear stability theory of two-layer fluid flow in an inclined channel, Physics of Fluids 6 (1994) 3906–3922.

[7] M. G. Blyth, C. Pozrikidis, Effect of surfactants on the stability of two-layer channel flow, Journal of Fluid Mechanics 505 (2005) 59–86.

[8] W. Y. Jiang, B. Helenbrook, S. P. Lin, Inertialess instability of a two-layer liquid film flow, Physics of Fluids 16 (2004) 652–663.

[9] J. Thompson, M. G. Blyth, Inertialess multilayer film flow with surfactant: Stability and traveling waves, Physical Review Fluids 1 063904.

[10] K. D. Danov, V. N. Paunov, N. Alleborn, H. Raszillier, F. Durst, Stability of evaporating two-layered liquid in the presence of surfactant – I. The equations of lubrication approximation, Chemical Engineering Science 53 (1998) 2809–2822.

[11] N. R. Anturkar, T. C. Papanastasiou, J. O. Wilkes, Lubrication theory for n-layer thin-film flow with applications to multilayer extrusion and coating, Chemical Engeering Science 45 (1990) 3271–3282.

[12] H. Schlichting, K. Gersten, Boundary-Layer Theory, Springer, 2000.

[13] V. Y. Shkadov, Wave Flow Regimes of a Thin Layer of Viscous Fluid Subject to Gravity, Fluid Dynamics 2 (1967) 29–34. doi:10.1007/BF01024797.

[14] D. J. Benney, Long waves on liquid films, Journal of Mathematical Physics 45 (1966) 150–155.

[15] K. J. Ruschak, S. J. Weinstein, Developing Film Flow on an Inclined Plane With a Critical Point, Journal of Fluids Engineering 123 (2001) 698–709.

[16] S. J. Weinstein, K. J. Ruschak, K. C. Ng, Developing flow of a power-law liquid film on an inclined plane, Physics of Fluids 15 (10) (2003) 2973–2986. doi:10.1063/1.1605742.

[17] C. Ruyer-Quil, P. Manneville, Improved modeling of flows down inclined planes, European Physical Journal B: Condensed Matter Physics 15 (2000) 357–369.

[18] S. Kalliadasis, A. Kiyashko, E. A. Demekhin, Marangoni instability of a thin liquid film heated from below by a local heat source, Journal of Fluid Mechanics 475 (2003) 377–408. doi:10.1017/S0022112002003014.

[19] S. Kalliadasis, E. A. Demekhin, C. Ruyer-Quil, M. G. Verlarde, Thermocapillary instability and wave formation on a film falling down a uniformly heated plane, Journal of Fluid Mechanics 492 (2003) 303–338.

[20] E. D. Kay, S. Hibberd, H. Power, A depth-averaged model for non-isothermal thin-film rimming flow, International Journal of Heat and Mass Transfer 70 (2014) 1003–1015. doi:http://dx.doi.org/10.1016/j.ijheatmasstransfer.2013.11.040.

[21] A.-J.-C. B. de Saint-Venant, Théorie du mouvement non permanent des eaux, avec application aux crues des rivières et à l´introduction des marées dans leur lit, Comptes rendus de l´Académie des Sciences.

[22] R. Manning, On the flow of the flow in water in open channels and pipes, Trans. I.C.E. Ireland 20 (1891) 161–207.

[23] M. F. Gobbi, J. T. Kirby, Wave evolution over submerged sills: tests of a high-order Boussinesq mode, Coastal Engineering 37 (1999) 57–96.

[24] P. Lynett, L.-F. Liu, P, A two-layer approach to wave modelling, Proceedings of the Royal Society of London Series A 460 (2004) 2637–2669.

[25] P. Lynett, L.-F. Liu, P, Linear analysis of the multi-layer model, Coastal Engineering 51 (2004) 439–454.

[26] E. Audusse, M. O. Bristeau, M. Pelanti, J. Sainte-Marie, Approximation of the hydrostatic Navier-Stokes system for density stratified flows by a multilayer model: Kinetic interpretation and numerical solution, Journal of Computational Physics 230 (2011) 3453–3478.

[27] E. Audusse, F. Benkhaldoun, S. Sari, M. Seaid, P. Tassi, A fast finite volume solver for multi-layered shallow water flows with mass exchange, Journal of Computational Physics 272 (2014) 23–45.

[28] C. B. Vreugdenhill, Two-Layer Shallow-Water Flow in Two Dimensions, a Numerical Study, Journal of Computational Physics 33 (1979) 169–184.

[29] E. Audusse, M. O. Bristeau, A. Decoene, Numerical simulation of 3d free surface flows by a multilayer Saint-Venant model, International Journal for Numerical Methods in Fluids 56 (2008) 331–350.

[30] D. Berghezan, F. Dupret, Numerical Simulation of Stratified Coating Flow by a Variational Method, Journal of Computational Physics 111 (1994) 165–182.

[31] F. Denner, B. G.M. van Wachem, Numerical time-step restrictions as a result of capillary waves, Journal of Computational Physics 285 (2015) 24–40.

[32] E. D. Kay, S. Hibberd, H. Power, Inertial effects at moderate Reynolds number in thin-film rimming flows driven by surface shear, Physics of Fluids 25 (2013) 102108. doi:10.1063/1.4825134.

[33] F. M. White, Fluid Mechanics, 6th Edition, McGraw-Hill, 2008.

[34] E. Y. Gatapova, O. A. Kabov, Shear-driven flows of locally heated liquid films, International Journal of Heat and Mass Transfer 51 (2008) 4797–4810. doi:10.1016/j.ijheatmasstransfer.2008.02.038.